BoBBLE: ocean-atmosphere interaction and its impact on the South Asian monsoon

Article

Accepted Version

BoBBLE (Bay of Bengal Boundary Layer Experiment): Ocean–atmosphere interaction and its impact on the South Asian monsoon

P. N. Vinayachandran*

Centre for Atmospheric and Oceanic Sciences, Indian Institute of Science, Bangalore 560 012, India

Adrian J. Matthews

Centre for Ocean and Atmospheric Sciences, School of Environmental Sciences and School of Mathematics, University of East Anglia, Norwich, UK

K. Vijay Kumar

CSIR-National Institute of Oceanography, Goa, India

Alejandra Sanchez-Franks

National Oceanography Centre, Southampton, UK

V. Thushara, Jenson George

Centre for Atmospheric and Oceanic Sciences, Indian Institute of Science, Bangalore, India

V. Vijith

Centre for Atmospheric and Oceanic Sciences, Indian Institute of Science, Bangalore, India,

Present affiliation: School of Marine Sciences, Cochin University of Science and Technology, Kochi, India

Benjamin G. M. Webber, Bastien Y. Queste

Centre for Ocean and Atmospheric Sciences, School of Environmental Sciences, University of East Anglia, Norwich, UK

Rajdeep Roy

Indian Space Research Organisation, National Remote Sensing Centre, Hyderabad, India

Amit Sarkar

ESSO-National Centre for Antarctic and Ocean Research, Goa, India

Dariusz B. Baranowski

Institute of Geophysics, Faculty of Physics, University of Warsaw, Poland

G. S. Bhat

Centre for Atmospheric and Oceanic Sciences, Indian Institute of Science, Bangalore, India

Nicholas P. Klingaman, Simon C. Peatman

National Centre for Atmospheric Science – Climate, University of Reading, UK

C. Parida

Berhampur University, Odisha, India

Karen J. Heywood, Robert Hall

Centre for Ocean and Atmospheric Sciences, School of Environmental Sciences, University of East Anglia, Norwich, UK

Brian King, Elizabeth C. Kent

National Oceanography Centre, Southampton, UK

Anoop A. Nayak, C. P. Neema

Centre for Atmospheric and Oceanic Sciences, Indian Institute of Science, Bangalore, India

P. Amol

CSIR-National Institute of Oceanography, Visakhapatnam, India

A. Lotliker

ESSO-Indian National Centre for Ocean Information Services, Hyderabad, India

A. Kankonkar, D. G. Gracias, S. Vernekar, A. C. D.Souza

CSIR-National Institute of Oceanography, Goa, India

G. Valluvan

ESSO-National Institute of Ocean Technology, Chennai, India

Shrikant M. Pargaonkar

Centre for Atmospheric and Oceanic Sciences, Indian Institute of Science, Bangalore, India

K. Dinesh

ESSO-Indian National Centre for Ocean Information Services, Hyderabad, India

Jack Giddings, Manoj Joshi

Centre for Ocean and Atmospheric Sciences, School of Environmental Sciences, University of East Anglia, Norwich, UK

Corresponding author address: P. N. Vinayachandran, Centre for Atmospheric and Oceanic Sciences, Indian Institute of Science, Bangalore 560 012, India

E-mail: vinay@iisc.ac.in

ABSTRACT

The Bay of Bengal (BoB) plays a fundamental role in controlling the weather systems that make up the South Asian summer monsoon system. In particular, the southern BoB has cooler sea surface temperature (SST) that influence ocean–atmosphere interaction and impact on the monsoon. Compared to the southeast, the southwestern BoB is cooler, more saline, receives much less rain, and is influenced by the Summer Monsoon Current (SMC). To examine the impact of these features on the monsoon, the BoB Boundary Layer Experiment (BoBBLE) was jointly undertaken by India and the UK during June – July 2016. Physical and bio-geochemical observations were made using a CTD, five ocean gliders, a uCTD, a VMP, two ADCPs, Argo floats, drifting buoys, meteorological sensors and upper air radiosonde balloons. The observations were made along a zonal section at 8°N between 85.3°E and 89°E with a 10-day time series at 89°E, 8°N. This paper presents the new observed features of the southern BoB from the BoBBLE field program, supported by satellite data. Key results from the BoBBLE field campaign show the Sri Lanka Dome and the SMC in different stages of their seasonal evolution and two freshening events during which salinity decreased in the upper layer leading to the formation of thick barrier layers. BoBBLE observations were taken during a suppressed phase of the intraseasonal oscillation; they captured in detail the warming of the ocean mixed layer and preconditioning of the atmosphere to convection.

Capsule Summary: A field experiment in the southern Bay of Bengal to generate new high-quality in situ observational data sets of the ocean, air–sea interface and atmosphere during the summer monsoon.

1. Introduction

The Bay of Bengal (BoB) holds a prominent place in the science of monsoons owing to its impacts on the South Asian summer monsoon rainfall and its variability over the countries located along the rim of the BoB, which is home to over a billion people. Maximum rainfall during the summer monsoon is received in the northeastern BoB and the adjoining land area (Xie et al. 2006). Weather systems that form over the BoB contribute substantially to rainfall over central India (Gadgil 2003). Several such systems breed over the BoB during each monsoon season because of the capacity of the BoB to recharge its sea surface temperature (SST) quickly in the short sunny spells after the passage of each disturbance (Shenoi et al. 2002; Bhat et al. 2001). This rapid SST warming is facilitated by the thin mixed layer maintained by freshwater input from rainfall and river runoff into the BoB (Vinayachandran et al. 2002). These general features characterise the BoB north of about 15°N.

Further south, features of the ocean-atmosphere system are somewhat different (Mathews et al., 2015, CLIVAR Exchanges, 19(3), 38-42), yet intriguing. Climatologically, both the ocean and atmosphere show contrasts between east and west. The SST is marked by a cold pool (Joseph et al. 2005; Das et al. 2016) around Sri Lanka (Fig. 1a) compared to the warmer water in the east. The sea surface salinity (SSS; Fig. 1b) is higher in the west than in the east (Vinayachandran et al. 2013). Most remarkably, the western part of the southern BoB is marked by the intense monsoon current that flows into the BoB carrying higher salinity Arabian Sea water. The atmosphere above the cold pool is characterized by a minimum in seasonal total rainfall (Fig. 1a) and has the lowest amount of low level clouds in the region (Shankar et al. 2007; Nair et al. 2011). The role of ocean dynamics and air–sea interaction processes in defining these large zonal and meridional variations, and the impact of these on monsoon rainfall elsewhere, have received little attention.

Several field experiments have been conducted in the BoB to understand the response of the BoB to monsoons and its possible feedbacks (Bhat and Narasimha 2007). Among the recent experiments, BOBMEX (Bay of Bengal Monsoon Experiment; Bhat et al. (2001)) focused on the coupled ocean–atmosphere system in the northern BoB during the peak monsoon months of July–September. The JASMINE (Joint AirSea Monsoon Interaction Experiment) sampled the eastern Indian Ocean and southern BoB during May and September, 1997 (Webster et al. 2002). The CTCZ (Continental Tropical Convergence Zone) experiment carried out under the Indian Climate Research Program made observations of both the southern and northern BoB during 2009 and 2012 (Rao et al. 2011; Vinayachandran et al. 2013; Jain et al. 2016). The ASIRI (Air-Sea Interactions Research Initiative) campaign covered both summer and winter monsoons and combined data sets from multiple platforms and model simulations (Wijesekera et al. 2016b). These experiments have contributed significantly towards our understanding of the processes at work during monsoons, but a large gap exists in our knowledge base about the physical processes in the southern BoB. BoBBLE focuses on the less known, yet important, southern BoB and combines observations from multiple instruments including five ocean gliders to obtain high-quality time series observations of the ocean, air–sea interface and atmosphere during the peak period of the 2016 summer monsoon.

The first set of measurements in the region was carried out by Schott et al. (1994) using current meter moorings and ship sections in the early nineties, which provided a description of the annual cycle and intraseasonal variation of monsoon currents. Earlier hydrographic surveys (Murty et al. 1992) indicated the flow of high salinity water into the southern BoB. The intrusion of the Summer Monsoon Current (SMC) into the BoB was described using geostrophic currents derived from Expendable bathythermograph (XBT) data sets (Vinayachandran et al. 1999). The seasonal cycle and interannual variability of the thermocline along 6°N was explored using the XBT data (Yu 2003). Using ship-board observations made during the CTCZ field campaign, Vinayachandran

et al. (2013) described the existence of a salt pump in the southern BoB. Using ADCP moorings, Wijesekera et al. (2016c) obtained current measurements from east of Sri Lanka for nearly two years. Lee et al. (2016) reported observations using multiple platforms, towards understanding the circulation and transport around Sri Lanka. Sustained ocean observation systems, RAMA McPhaden et al. (2009) in particular, have also contributed to the data base in this region. However, there is a major gap in the observations that are relevant to understanding the complete ocean–atmosphere system during the summer monsoon.

The primary objective of the BoBBLE field program was to characterize the ocean–atmosphere system in the southern BoB, which is marked by contrasting features in its east and west. One of the major aims is to generate new high-quality in situ observational data sets of the ocean, air–sea interface and atmosphere during the peak phase of the summer monsoon. The overarching objectives of BoBBLE are to evaluate the role of ocean–atmosphere interactions in the simulation and prediction of the summer monsoon, to combine data and models to investigate the physical and bio-geochemical processes under the monsoon forcing, and to determine the role of the above mentioned processes in causing the synoptic-scale variability of the south Asian monsoon system.

The aim of this paper is to make the community aware of the new data set that has been acquired, and to present a preliminary analysis of the observations collected during the BoBBLE field program, the details of which are given in section 2. Sections 3 and 4 describe air–sea interaction, and the oceanographic features of the southern BoB, respectively. We conclude with a summary and outlook in section 5.

2. BoBBLE field program

The research vessel *RV Sindhu Sadhana* (Fig. 2), sailed from the port of Chennai on 24 June and returned on 23 July 2016. The BoBBLE cruise was conducted along the track shown in Fig. 3.

Ship-board observations can be classified into two types: observations made along the 8°N section from 85.3°E to 89°E, in the international waters of the southern BoB and time series observations were at 89°E, 8°N (hereafter referred to as TSE) for a period of 10 days, 4–15 July 2016. Ocean glider deployments provided similar time series at locations marked as black circles in Fig. 3.

Two ship-board Acoustic Doppler Current Profilers (ADCP, operating at frequencies of 38 kHz and 150 kHz), an autonomous weather station (AWS) and a thermo-salinograph recorded data continuously during the cruise period. A SeaBird Electronics (SBE) 9/11+ Conductivity-Temperature-Depth profiler (CTD) measured vertical profiles and collected water samples at all points marked as stars in Fig. 3. Nominally, the casts were to a depth of 1000 m. At selected stations, additional CTD casts extended all the way to the deep ocean floor. At TSE, CTD observations were carried out to a depth of 500 m at approximately 3-hourly intervals, with a once-daily profile to 1000 m. Four standard MetOcean drifting buoys were also deployed during the BoBBLE field program.

Five ocean gliders were deployed during 1-19 July 2016 along the 8°N transect (Table 1). All gliders were equipped with a CTD package, enabling measurements of temperature and salinity with 0.5–1 m vertical resolution from the surface to 1000 m depth. Four gliders were equipped with dissolved oxygen (dO2), chlorophyll fluorescence (Chl) and optical backscatter sensors. Additionally, one glider (SG579) was equipped with a photosynthetically active radiation (PAR) sensor, and another (SG613) with microstructure shear and temperature sensors. Individual dives lasted 3–4 hours. In total, 462 dives were made. Optimally interpolated (OI) two-dimensional (depth, time) gridded data sets (Matthews et al. 2014) were produced for each glider. The radii of influence in the Gaussian weighting functions were 2 m and 3 hr, respectively. The five depth–time OI data sets were then further combined into a single three-dimensional longitude–depth–time data set, by linear interpolation in longitude, taking account of the movement of the gliders with time.

Seven Argo floats were deployed in the BoB along 8°N, between 85.3°E and 89°E (Table 2). As BoBBLE is designed to target surface processes, all floats were programed to provide daily high-resolution profiles of the top 500 m in a region where in situ surface data are scarce. A second OI data set was created using profiles from core Argo floats from the international Argo program, BoBBLE Argo floats, glider profiles and the shipboard CTD. These OI data were mapped using World Ocean Atlas climatology (Boyer et al. 2013) and gridded at 25 longitude grid points at 8°N, from 83°E to 95°E at 0.5° intervals. The time grid ran from 1 June 2016, before the BoBBLE field campaign started, to 30 September 2016, with data from each day gridded separately. This combined OI data set covers a longer time period than the BoBBLE field program, as there was a continuous Argo float presence in the BoB, before BoBBLE campaign which was then significantly enhanced by the seven floats deployed during BoBBLE.

To map mesoscale and sub-mesoscale features, an Ocean Sciences–Teledyne underway CTD (uCTD), fitted with SBE CT sensors, was used for measuring temperature and salinity profiles while the ship was sailing at a speed of 6 knots. Nominally, the uCTD probe was allowed to profile vertically for 2 minutes in order to achieve a drop rate of about 1.5–2.5 m s^{-1} covering a depth range of approximately 250 m and the data was binned at 1m depth intervals.

A vertical microstructure profiler (Rockland Scientific VMP-250) comprising two shear probes, one set of high-resolution micro-temperature and conductivity sensors and another set of standard CTD sensors was operated at all glider stations along the transect as well as at TSE. At each station, 2–3 profiles were measured. At TSE, profiles were measured at 0000, 0400, 0800, 1200, and 1700 UTC each day. In total, 138 casts were made, including that at TSE.

To characterize the surface and sub-surface light field, bio-optical measurements were carried out with a Satlantic HyperProII hyperspectral underwater radiometer (HUR) equipped with three sensors for light, ECO triplet for fluorescence and colored dissolved organic matter (CDOM), and

CTD sensors. The light sensors measured downwelling, upwelling and total solar irradiance. The HUR was operated for 17 days under cloud-free conditions between 0600 and 0700 hrs UTC at TSE, and along the 8°N transect between 0530 and 0800 hrs UTC. A total of 37 profiles were collected during BoBBLE. An inherent optical profiler (IOP) was used for the measurement of light absorption and scattering coefficients, backscattering coefficient, chlorophyll-a, CDOM, turbidity and photosynthetically available radiation (PAR) along with a CTD sensor. The IOP was operated at TSE at 0130 and 0830 UTC each day.

The meteorological measurements included an AWS, air-sea flux observing system (Table 3), and radiosondes. A LI-COR, infrared gas analyzer in conjunction with the 3D sonic anemometer based eddy covariance system, along with high-frequency response ship motion sensors were installed at the bow, at a height of approximately 15 m above sea surface and 6 m above the forecastle deck. Sensible and latent turbulent heat fluxes are estimated using the eddy covariance method (Fairall et al. 1997; Edson et al. 1998; Dupuis et al. 2003). Upper air observations of temperature, pressure, humidity, and wind were taken with Vaisala RS92 radiosondes, launched nominally at 0000 UTC and 1200 UTC every day. Additional launches were also made on some days to capture the diurnal cycle.

3. Meteorology and air–sea interaction

a. Large-scale conditions over the BoB during summer 2016

The all-India rainfall for 2016 was 3% deficit relative to climatology (www.imd.gov.in), ENSO conditions were near neutral and SST anomalies in the tropical Pacific and Indian oceans were modest (www.ospo.noaa.gov). The Indian Ocean dipole (Saji et al. 1999) was in a negative state, with slightly warmer than usual conditions in the eastern Indian Ocean and cooler than usual con-

ditions in the west, representing an intensification of the usual cross-basin gradient. Despite this, the 2016 can be seen as a representative monsoon and is therefore ideally suited for investigating its link with conditions in the BoB.

The mean monsoon winds during the observation period were steady southwesterlies (Fig. 1d) and the SMC was intense with an axis oriented in the SW–NE direction, to the east of Sri Lanka (Fig. 1c). The mean SST was relatively cooler around the SMC with warmer water farther in the west and east. The east-west SST contrast that is typically seen in the climatology (Fig. 1a) was not as well developed during the period of observations (Fig. 1c). The mean SSS pattern was comparable to climatology (Fig. 1b,d).

Intraseasonal variability had a significant effect on the conditions observed during the BoBBLE campaign. In June 2016, the southern BoB was under the influence of a convectively active phase (Fig. 4) of the Boreal Summer Intraseasonal Oscillation (BSISO) (Lee et al. 2013). This propagated northward (dashed blue line in Fig. 4) and was replaced by a convectively suppressed phase of the BSISO during July 2016. Toward the end of the deployment, conditions returned to convectively active phase, with the incursion of the next cycle of the BSISO. Hence, the main BoBBLE deployment sampled the transition between the end of one active BSISO event, the subsequent suppressed phase and the initiation of the active phase in the following BSISO event. This is an ideal framework for analyzing the high-resolution in situ observations made during the BoBBLE cruise.

b. In situ measurements of air–sea interaction

The time series of surface fluxes and atmospheric and ocean surface conditions observed from the ship are described here, within the large-scale context of the suppressed phase of the BSISO in the southern BoB. The focus is on the 4–15 July 2016 period when the ship was at TSE location

at 89°E, 8°N (Fig. 5a). During this period, no precipitation was observed. Cloud conditions were characterized by broken layers of middle and high-level clouds and scattered small cumulus, with generally high surface solar radiation flux. The surface wind speeds during the first half of the period were 8–10 m s^{-1} (Fig. 5d), typical for the southern BoB during the summer monsoon. However, in the latter half of the period, they decreased to 5 m s^{-1} or below, with an associated reduction in the (cooling) surface latent heat flux.

The high solar radiation flux and relatively low latent heat flux are consistent with conditions that prevail during the suppressed (calm, clear) phase of the BSISO (Lee et al., 2013). Consequently, the net heat flux into the ocean was positive (Fig. 5e). This led to a steady increase in SST, from 28.0 to 29.5°C (Fig. 5b), again consistent with the developing oceanic conditions typically found in the suppressed BSISO phase. Surface atmospheric temperature (Fig. 5c) increased in pace with the SST.

Deep atmospheric convection broke out at the end of the TSE period. From 16 July 2016 onwards, deep convective cloud systems with intense precipitation, associated with the next active BSISO phase, were observed from the ship. It should be noted that at this time, the ship had departed TSE and was cruising westwards on the return leg of the 8°N section (Fig. 5a), hence the sampling of these precipitating systems was not at a fixed location. This deep convection was part of the next active BSISO phase (Fig. 4).

The change in atmospheric characteristics from suppressed to active convection can clearly be seen in the shipboard AWS time series. The most notable change is that air temperature dropped on 15 July and remained significantly lower than SST from then on (Fig. 5b,c). The air temperature was much more variable, with spikes of low temperature followed by gradual recovery. Low temperature spikes are due to the evaporation from falling rain drops in the sub-cloud layer and formation of a pool of cold air near the surface (i.e., wet bulb effect). Surface wind speed increases

from its minimum on 15 July (Fig. 5d), and shows large variability. These are also likely due to gusts of cold, dry air originating from the convective systems associated with the transition to an active phase of BSISO.

Overall, the shipboard measurements comprehensively captured the transition from the atmospheric convectively suppressed phase of the BSISO during 4–15 July to the following convectively active phase.

Glider measurements extend the analysis of air-sea interaction along the entire 8°N section. The longitude–time section of ocean temperature at 1 m depth (Fig. 6a) clearly shows the gradual warming across the whole section from approximately 28.5°C on 3 July to up to 30.5°C on 13 July. Superimposed on this are strong diurnal fluctuations, especially at the westernmost glider (SG579) and 88°E (SG532). These represent the formation of surface diurnal warm layers (Fig. 6b), previously diagnosed in the Indian Ocean by an ocean glider (Matthews et al. 2014).

Argo floats extend the analysis even further to the end of the season. With the onset of the next active phase of BSISO in mid July, the temperature rapidly decreased (Fig. 6c) followed by a weaker warming from mid-August to mid-September and a further cooling.

4. Oceanographic features of the southern BoB

The deployment of multiple platforms has yielded an unprecedented description of the oceanographic features of the southern BoB during the summer monsoon. In particular, a nearly one-month time series of physical and bio-geochemical variables along a zonal section at 8°N has been obtained. This section describes these features briefly.

a. Sri Lanka Dome (SLD)

The cyclonic circulation feature located to the east of Sri Lanka, caused by cyclonic wind stress curl above the SLD (Fig7a), associated with doming of the thermocline is known as the SLD (Vinayachandran and Yamagata (1998); Wijesekera et al. (2016a)). The SLD during BoBBLE is seen as a patch of negative mean sea level anomalies (MSLA; Fig. 7a), enclosed by the zero MSLA contour (thick line). The SLD was well developed during the survey with cyclonic circulation and cooler SST around it (Fig 7b). The CTD profiles measured during BoBBLE captured the doming of the thermocline with respect to its exterior. On 28 and 30 June 2016, CTD profiles were measured at locations within the SLD, and on 01 July 2016, on its outer edge. A comparison of these profiles shows that the thermocline (taken as the depth of the 20°C isotherm; D20) within the dome is about 30 m shallower compared to its exterior (Fig. 7c). The dome also shows distinct salinity characteristics (Fig. 7d). The sub-surface high salinity core that exists along with the SMC (section 4c) does not penetrate into the SLD. The near-surface salinity within the SLD is higher compared to the north but lower than that in the east, confirming its isolation from the influence of the SMC.

Along 8°N (Fig. 8), the thermocline (D20) within the dome is elevated relative to the region to the east. The CTD and glider sections in early July (Fig. 8a,b) corresponds well during the season. The SLD moves westward as the season progresses (Fig. 8c). It has been possible to delineate the changes in the east–west slope of the thermocline from early to mid July because of these data sets generated by multiple instrumentation (Fig. 8d).

b. The Summer Monsoon Current

The SMC flows eastward to the south of India (Schott et al. 1994) and then turns to flow into the BoB (Murty et al. 1992; Vinayachandran et al. 1999, 2013). The SMC was fully developed

during the observation period with near-surface speeds of 0.5–1 m s^{-1} (Fig. 9a,b). The circulation was characterized by a large cyclonic gyre to the east of Sri Lanka, that was fully developed by the last week of June (Fig. 9a). The main axis of the SMC that flows northeastward into the BoB weakened and moved westwards by mid-July; in the process, the gyre elongated and shrank. Multiple filaments emanated from the SMC in different directions (Fig. 9b). One of them flowed towards the equator, another towards the east, one towards the northeast and another continued to the southeast. One of the drifting buoys deployed during the cruise at TSW (Fig. 3) on 29 June traversed along the cyclonic gyre (Fig. 9c) but two drifters continued towards India. The drifter deployed in the east (147132; Fig. 9c) moved southeast.

The BoBBLE section cut across the main branch of the SMC, and the TSE location was located on the outer edge of the filament flowing to the northeast. Geostrophic currents (Fig. 9d) showed high speeds (> 0.5 m s^{-1}) near the surface and the northward flow was restricted to depths shallower than 200 m in agreement with previous observations (Wijesekera et al. 2016a). ADCP profiles confirm the shallow nature of the SMC (Fig. 9e,f). Between the two visits, the SMC weakened and shifted westwards, the latter being consistent with the well-known process of Rossby wave propagation across the BoB (McCreary et al. 1996; Shankar et al. 2002). There is a remarkable agreement between the ADCP data and geostrophic currents. The time-depth section of the geostrophic component of the SMC derived from glider data (Fig. 9e,g)show decreasing velocities, consistent with the weakening and westward propagation of the SMC.

c. The high salinity core

The SMC carries high salinity water (> 35.2 psu) from the Arabian Sea into the BoB. On encountering the lighter water of lower salinity, the Arabian Sea water subducts beneath the latter. The intrusion of high salinity (35 to 35.6 psu) water occurs below the mixed layer, to a maximum

depth of about 200 m (Fig. 10). During 30 June to 4 July (Fig. 10a), the high salinity core was confined to 86–89°E, between 25–175 m depth. At the eastern end (at 89°E), the core thinned to about 25 m thickness. In contrast, at the western end, the profiles measured inside the SLD did not show the presence of Arabian Sea water (Fig. 7d). At TSE, (Fig. 10b) the core thickened from about 25 m on 4 July to about 100 m on 15 July suggesting a steady supply of high salinity water during the observation period. Glider (Fig. 10d) and Argo (Fig. 10e) observations reveal temporal variations of the high salinity core along the 8°N section.

d. Freshening events and barrier layer formation

The 10-day time series at TSE captured two freshening events, one during 4–6 July and the other during 8–9 July (Fig. 10c). These events led barrier layers to form between the base of the upper isohaline layer and the base of the isothermal layer. The barrier layer formed rapidly during the first event. The SSS on 4 July dropped by 0.3 in 2 hours, decreasing from 34.3 psu at 0530 UTC to 33.9 psu by 0730 UTC (Fig. 11). Since there was no rain locally, this drop in salinity is attributed to horizontal advection. The mixed layer depth (MLD) decreased from 70 m to 18 m leading to the formation of a barrier layer that was about 50 m thick and had a temperature of 29°C. The upper layer warmed by about 0.3°C relative to the barrier layer below, during the following diurnal cycle.

The second event occurred more gradually; the SSS (MLD) decreased from 34.40 psu (75m) on 07 July to 33.57 psu (35m) on 13 July (Fig. 11). Consequently, a new barrier layer formed that was about 40 m thick. Periods of low SST coincided with higher salinity and the SST increased after both freshening events. There was also a distinct increase in the diurnal warming of SST after the freshening.

The barrier layer formation at TSE is comparable to that in the northern bay where the influence of river runoff and rainfall is more intense. Subsequent to the arrival of a fresh plume, the MLD

decreased from 30 to 10 m during the 1999 summer monsoon (Vinayachandran et al. 2002), as a result of the decrease in SSS by about 4 psu over a period of 7 days. Observations during 2009 (Rao et al. 2011) also showed a similar decrease of SSS and MLD in one day. It is quite remarkable that even in the southern bay, where the direct influence of fresh water is much weaker compared to that in the north, the mixed layer shallowing and barrier layer formation occur to a comparable degree, suggesting that the behavior of the southern BoB mixed layer is comparable to that of the north during the summer monsoon.

e. Sub-mesoscale observations

A uCTD was used for measuring vertical profiles of temperature and salinity, while the ship was in transit (details in section 2). A uCTD section measured just after a spell of rain near TSE on 15 July 2016 (Fig. 12a) captured the spatial scale of a low salinity pool formed due to the rain event. The salinity within the fresh pool was lower by 0.1 psu compared to the region outside, and the impact of rain was seen to a depth of 12 m. The width of this pool was 7 km. There was no apparent change in the temperature (Fig. 12b) and the isothermal layer extended all the way to about 40 m despite the isohaline layer being confined to the upper 10 m.

f. Microstructure measurements

Previous indirect dissipation measurements inferred from Argo floats in the central BoB suggested very low dissipation rates in the 250–500 m depth range (Whalen et al. 2012). Recent direct dissipation measurements in the northern and central BoB (Jinadasa et al. 2016) show that the pycnocline is mostly decoupled from the low salinity surface layer, with low turbulence in the deeper layer. Profiles from simultaneous casts of the VMP-250 (Fig. 13a-c) and the microstructure glider (Fig. 13d-f) at locations separated by a few kilometre suggest a shallow mixed layer

(approximately 20 m thick) and a freshened upper layer (33.5 psu) compared to the thermocline region where salinity is 35.25 psu, confirming that the two platforms are sampling similar water columns. The 3 m binned profiles of turbulent kinetic energy dissipation rate (ε) and vertical diffusivity (K_z) from the VMP (Fig. 13c) and the microstructure glider (Fig. 13f) suggest a sporadic and intermittent nature of the mixing in the water column. Within the mixed layer, the ε and K_z were greater than 10^{-8} W kg^{-1} and 10^{-4} m^{2}s^{-1}, respectively. Below the mixed layer, ε decreased to 10^{-10} W kg^{-1}, and K_z reduced to 10^{-6} m^{2}s^{-1}. The microstructure data are consistent with the observations of Jinadasa et al. (2016) and Whalen et al. (2012).

g. Biogeochemical observations

Light Penetration and Chlorophyll

The glider SG579 (Table 1.) equipped with a PAR sensor provides a proxy for the shortwave radiation flux. A sample profile (Fig. 14) shows a rapid decrease in radiation flux in the top 1–2 m, associated with the absorption of the red light part of the spectrum. Below this level, PAR decreases much more slowly, associated with absorption of the blue light part of the spectrum. A double exponential curve was fitted, producing a scale depth of 0.3 m for red light, and 18 m for blue light. Co-located measurements of chlorophyll concentration (Table 1.) show a layer of chlorophyll below 30 m (green line in Fig. 14), with near zero values above this. The effects of chlorophyll absorption of solar radiation, and any subsequent effect on SST, and through ocean–atmosphere interactions, a feedback onto precipitation, will be examined during the project.

O2 and pCO_2

The dissolved oxygen at the surface ranged between 199–212 μM/Kg with the eastern part of the transect showing relatively higher values (Fig. 15a). The surface pH (Fig. 15b), total alkalinity (Fig. 15c) and pCO_2(Fig. 15e) exhibited a similar distribution. The pH had a range of 8.071–

8.168 units, whereas total alkalinity varied between 2172–2295 μmol kg^{-1}. Atmospheric CO_2 (pCO_2^{air}) ranged between 386–409 μatm (Fig. 15d), where higher concentrations were associated with the AR station at 85.3°E, 10°N (Fig. 3). This station also exhibited high pCO_2 (sea water) with a range of 467–554 μatm. The low surface pH in tandem with low alkalinity and high pCO_2 at this station suggest upwelled waters, presumably associated with the SMC. Overall, all sampling stations exhibited high pCO_2 compared to the atmospheric mixing ratios, suggesting that the southern BoB is a possible source of CO_2 to the atmosphere during summer.

5. Summary and outlook

During a typical summer monsoon season, discrete cloud bands periodically form over the Indian Ocean and then migrate over the Asian land mass, culminating in rainfall there. Such cloud bands can be embedded in large-scale intraseasonal oscillations or manifest as synoptic monsoon depressions. The BoB is a key region for the formation and propagation of these atmospheric systems. Thus, the variability of rainfall over the Asian land mass during the monsoon is closely linked to the exchange of heat and moisture taking place over the Indian Ocean. Hence, understanding the detailed physical processes of ocean–atmosphere interaction over the Indian Ocean, and the BoB in particular, is crucial for understanding and successful modeling and prediction of monsoon variability.

BoBBLE was motivated by this need and designed to investigate oceanographic conditions and air–sea interaction over the hitherto little known southern BoB during the summer monsoon. This paper outlines the preliminary results from the BoBBLE field program, which was aimed at collecting high-quality in situ observations from multiple platforms, including an ocean research ship, five ocean gliders, and seven specially configured Argo floats.

The BoBBLE observations were made during July 2016, during a suppressed phase of the BSISO when the ocean and atmosphere were being pre-conditioned for an impending active stage of the monsoon. During this period, which was characterized by intense solar radiation, the ocean warmed, and exhibited strong diurnal variability. At the end of the BoBBLE observation period, atmospheric convection broke out over the southern BoB as part of the next, active phase of a northward-propagating BSISO. This active phase subsequently led to rainfall over India and the Asian land mass.

The BoBBLE campaign has also made detailed observations of the major oceanographic features of the southern BoB. Using multiple in situ platforms, the spatial and temporal evolution of features such as the SLD Dome and the high salinity core in the SMC have been delineated using in situ data sets. Other observations include the formation of barrier layers in the southern BoB, and details of the associated changes in the mixed layer. The physical processes involved in barrier layer formation in the southern BoB contrast with those at work in the north.

The next challenge for the BoBBLE program is to incorporate the observational knowledge gained by the field program into physical process models, and to determine the sensitivity of the monsoon system to ocean–atmosphere interactions in the southern BoB.

Acknowledgments. BoBBLE is a joint MoES, India–NERC, UK program. The BoBBLE field program on board *RV Sindhu Sadhana* was funded by Ministry of Earth Sciences, Govt. of India under its Monsoon Mission program administered by Indian Institute of Tropical Meteorology, Pune. We are indebted to CSIR-National Institute of Oceanography, Goa for providing their research ship *RV Sindhu Sadhana* for BoBBLE. Encouragements by Dr M. Rajeevan, Secretary, MoES and Dr S. S. C. Shenoi, Director INCOIS are greatly appreciated. The support and co-operation of Dr P. S. Rao (NIO), the Captain, officers and crew of *RV Sindhu*

Sadhana are greatly appreciated. We thank Dr. D. Shankar (NIO) Dr. R. Venkatesan (NIOT), Dr Tata Sudhakar (NIOT), Dr. Anil Kumar (NCOAR), Dr. M. Ravichandran (INCOIS) and their team, for their support for the field program. ASCAT winds were obtained from IFREMER (http://www.ifremer.fr/cersat/en/data/data.htm), NCEP from http://www.esrl.noaa.gov/psd/ (Kalney et al, 1996), CERES downward long wave and short wave from https://ceres.larc.nasa.gov, OSCAR from https://podaac.jpl.nasa.gov/CitingPODAAC, AMSR-E products from http://www.remss.com/missions/amsr, KALPANA-OLR from http://www.tropmet.res.in, TRMM-rainfall from http://daac.gsfc.nasa.gov/precipitation, MSLA from Copernicus Marine and Environment Monitoring Service (CMEMS) (http://www.marine.copernicus.eu), gridded Argo data from from Global Data Assembly Centre (Argo GDAC), SEANOE and ERA winds, fluxes and meteorological parameters from http://www.ecmwf.int/en/research/climate-reanalysis/era-interim. The core Argo profiles were collected and made freely available by the international Argo program and the national programmes that contribute to it (http://www.argo.ucsd.edu,http://argo.jcommops.org) NPK was supported by NERC (NE/L010976/1). ASF, BGMW and SCP were supported by the NERC BoBBLE project (NE/L013835/1, NE/L013827/1, NE/L013800/1).

.

References

Bhat, G. S., and R. Narasimha, 2007: Indian summer monsoon experiments. *Curr. Sci.*, **93 (2)**, 153–164.

Bhat, G. S., and Coauthors, 2001: BOBMEX: The Bay of Bengal monsoon experiment. *Bull. Am. Meteorol. Soc.*, **82 (10)**, 2217–2243.

Boyer, T. P., and Coauthors, 2013: Noaa atlas nesdis 72. *World Ocean Database*.

Das, U., P. N. Vinayachandran, and A. Behara, 2016: Formation of the southern Bay of Bengal cold pool. *Clim. Dyn.*, **47 (5-6)**, 2009–2023.

Dupuis, H., C. Guerin, D. Hauser, A. Weill, P. Nacass, W. M. Drennan, S. Cloché, and H. C. Graber, 2003: Impact of flow distortion corrections on turbulent fluxes estimated by the inertial dissipation method during the FETCH experiment on R/V L'Atalante. *J. Geophys. Res.: Oceans*, **108 (C3)**.

Edson, J. B., A. A. Hinton, K. E. Prada, J. E. Hare, and C. W. Fairall, 1998: Direct covariance flux estimates from mobile platforms at sea. *J. Atmos. Oceanic Technol.*, **15 (2)**, 547–562.

Fairall, C., A. White, J. Edson, and J. Hare, 1997: Integrated shipboard measurements of the marine boundary layer. *J. Atmos. Oceanic Technol.*, **14 (3)**, 338–359.

Gadgil, S., 2003: The Indian monsoon and its variability. *Annu. Rev. Earth Planet. Sci.*, **31 (1)**, 429–467.

Jain, V., and Coauthors, 2016: Evidence for the existence of Persian Gulf Water and Red Sea Water in the Bay of Bengal. *Clim. Dyn.*, 1–20.

Jinadasa, S. U. P., I. Lozovatsky, J. Planella-Morató, J. D. Nash, J. A. MacKinnon, A. J. Lucas, H. W. Wijesekera, and H. J. S. Fernando, 2016: Ocean turbulence and mixing around Sri Lanka and in adjacent waters of the northern Bay of Bengal. *Oceanography*, **29 (2)**, 170–179.

Joseph, P. V., K. P. Sooraj, C. A. Babu, and T. P. Sabin, 2005: A Cold Pool in the Bay of Bengal and its interaction With The Active-Break Cycle of Monsoon. *CLIVAR Exchanges*, **10 (3)**, 10–12.

Lee, C. M., and Coauthors, 2016: Collaborative observations of boundary currents, water mass variability, and monsoon response in the southern Bay of Bengal. *Oceanography*, **29 (2)**, 102–111.

Lee, J.-Y., B. Wang, M. C. Wheeler, X. Fu, D. E. Waliser, and I.-S. Kang, 2013: Real-time multivariate indices for the boreal summer intraseasonal oscillation over the Asian summer monsoon region. *Clim. Dyn.*, **40 (1-2)**, 493–509.

Matthews, A. J., D. B. Baranowski, K. J. Heywood, P. J. Flatau, and S. Schmidtko, 2014: The surface diurnal warm layer in the Indian Ocean during CINDY/DYNAMO. *J. Climate*, **27 (24)**, 9101–9122.

McCreary, J. P., W. Han, D. Shankar, and S. R. Shetye, 1996: Dynamics of the East India Coastal Current: 2. Numerical solutions. *J. Geophys. Res.: Oceans*, **101 (C6)**, 13 993–14 010.

McPhaden, M. J., and Coauthors, 2009: RAMA: The Research Moored Array for African-Asian-Australian Monsoon Analysis and Prediction. *Bull. Am. Meteorol. Soc.*, **90**, 459–480.

Moum, J. N., M. C. Gregg, R. C. Lien, and M. E. Carr, 1995: Comparison of turbulence kinetic energy dissipation rate estimates from two ocean microstructure profilers. *J. Atmos. Oceanic Tech.*, **12 (2)**, 346–366.

Murty, V. S. N., Y. V. B. Sarma, D. P. Rao, and C. S. Murty, 1992: Water characteristics, mixing and circulation in the Bay of Bengal during southwest monsoon. *J. Mar. Res.*, **50 (2)**, 207–228.

Nair, A. K. M., K. Rajeev, S. Sijikumar, and S. Meenu, 2011: Characteristics of a persistent pool of inhibited cloudiness and its genesis over the Bay of Bengal associated with the Asian summer monsoon. *Ann. Geophys.*, **29 (7)**, 1247–1252.

Osborn, T. R., 1980: Estimates of the local rate of vertical diffusion from dissipation measurements. *J. Phys. Oceanogr.*, **10 (1)**, 83–89.

Rao, S. A., and Coauthors, 2011: Modulation of SST, SSS over northern Bay of Bengal on ISO time scale. *J. Geophys. Res.*, **116 (C9)**.

Saji, N. H., B. N. Goswami, P. N. Vinayachandran, and T. Yamagata, 1999: A dipole mode in the tropical Indian Ocean. *Nature*, **401 (6751)**, 360–363.

Schott, F., J. Reppin, J. Fischer, and D. Quadfasel, 1994: Currents and transports of the Monsoon Current south of Sri Lanka. *J. Geophys. Res.*, **99 (C12)**, 25 127–25 141.

Shankar, D., S. R. Shetye, and P. V. Joseph., 2007: Link between convection and meridional gradient of sea surface temperature in the Bay of Bengal. *J. Earth. Syst. Sci.*, **116 (5)**, 385–406.

Shankar, D., P. N. Vinayachandran, and A. S. Unnikrishnan, 2002: The Monsoon current in the north Indian ocean. *Prog. Oceanogr.*, **52**, 63–120.

Shenoi, S. S. C., D. Shankar, and S. R. Shetye, 2002: Differences in heat budgets of the near-surface Arabian Sea and Bay of Bengal: Implications for the summer monsoon. *J. Geophys. Res.*, **107 (C6)**, 5–1.

Vinayachandran, P. N., Y. Masumoto, T. Mikawa, and T. Yamagata, 1999: Intrusion of the south-west monsoon current into the Bay of Bengal. *J. Geophys. Res.*, **104 (C5)**, 77–85.

Vinayachandran, P. N., V. S. N. Murty, and V. Ramesh Babu, 2002: Observations of barrier layer formation in the Bay of Bengal during summer monsoon. *J. Geophys. Res.: Oceans*, **107 (C12)**.

Vinayachandran, P. N., D. Shankar, S. Vernekar, K. K. Sandeep, P. Amol, C. P. Neema, and A. Chatterjee, 2013: A summer monsoon pump to keep the Bay of Bengal salty. *Geophys. Res. Lett.*, **40**, 1–6.

Vinayachandran, P. N., and T. Yamagata, 1998: Monsoon response of the sea around Sri Lanka: generation of thermal domesand anticyclonic vortices. *J. Phys. Oceanogr.*, **28 (10)**, 1946–1960.

Webster, P. J., and Coauthors, 2002: The JASMINE pilot study. *Bull. Am. Meteorol. Soc.*, **83 (11)**, 1603–1630.

Weller, R. A., E. F. Bradley, J. B. Edson, C. W. Fairall, I. M. Brooks, M. J. Yelland, and W. Pascal, Robin, 2008: Sensors for physical fluxes at the sea surface: energy, heat, water, salt. *Copernicus Publications on behalf of the European Geosciences Union*.

Whalen, C. B., L. D. Talley, and J. A. MacKinnon, 2012: Spatial and temporal variability of global ocean mixing inferred from Argo profiles. *Geophys. Res. Lett.*, **39 (18)**.

Wijesekera, H. W., W. J. Teague, D. W. Wang, E. Jarosz, T. G. Jensen, S. U. P. Jinadasa, H. J. S. Fernando, and Z. R. Hallock, 2016a: Low-frequency currents from deep moorings in the southern bay of bengal. *J. Phys. Oceanogr.*, **46 (10)**, 3209–3238.

Wijesekera, H. W., and Coauthors, 2016b: ASIRI: An Ocean–Atmosphere Initiative for Bay of Bengal. *Bull. Am. Meteorol. Soc.*, **97 (10)**, 1859–1884.

Wijesekera, H. W., and Coauthors, 2016c: Observations of currents over the deep southern Bay of Bengalwith a little luck. *Oceanography*, **29 (2)**, 112–123.

Xie, S.-P., H. Xu, N. H. Saji, Y. Wang, and W. T. Liu, 2006: Role of narrow mountains in large-scale organization of Asian monsoon convection. *J. Climate*, **19 (14)**, 3420–3429.

Yu, L., 2003: Variability of the depth of the 20°C isotherm along 6°N in the Bay of Bengal: Its response to remote and local forcing and its relation to satellite SSH variability. *Deep-Sea Res. II: Topical Studies in Oceanography*, **50 (12)**, 2285–2304.

554

555

556

LIST OF TABLES

TABLE 1. Ocean glider deployments during the BoBBLE cruise.

Glider ID	Waypoint	Deployed	Recovered	Instrumentation
SG579	8°N,86°E then 8°N,85°20′E	30 Jun	20 Jul	CTD, dO2, Chl, backscatter, PAR
SG534	8°N,87°E	1 Jul	17 Jul	CTD, dO2, Chl, backscatter
SG532	8°N,88°E	2 Jul	16 Jul	CTD, dO2, Chl, backscatter
SG620	8°N,88°54′E	3 Jul	14 Jul	CTD, dO2, Chl, backscatter
SG613	8°N,89°06′E	4 Jul	15 Jul	CTD, microstructure shear and temperature

TABLE 2. Argo float deployments during the BoBBLE cruise.

No.	Argo Float ID	Date	Time (UTC)	Lat	Lon	Notes
1	Navis OCR 0629	28/06/2016	11:45	8N	85.3E	Daily profile surfacing at 1200
2	Apex STS 7599	30/06/2016	09:10	8.04N	86.05E	Daily profile surfacing at 1500
3	Apex STS 7598	30/06/2016	09:10	8.04N	86.05E	Daily profile surfacing at 0300
4	Navis OCR 0631	01/07/2016	14:10	8.07N	87.04E	Daily profile surfacing at 1200
5	Apex STS 7597	01/07/2016	14:10	8.07N	87.04E	Daily profile surfacing at 1500
6	Apex STS 7596	02/07/2016	06:15	8N	88E	Daily profile surfacing at 1500
7	Navis OCR 0630	04/07/2016	13:23	8.06N	89.02E	Daily profile surfacing at 1200

TABLE 3. Details of ship-board meteorological instruments. Surface variables including air temperature (Ta), SST, relative humidity (RH), pressure, all four components of radiation, wind speed and direction, rain rate and ship position were continuously monitored by the AWS. Surface variables were sampled at 10-second intervals, and 1-minute averages (including true wind speed and direction) were stored. The ship's SBE SST sensor was placed at a depth of approximately 3.5 m below sea level (Weller et al. 2008).

Parameter	**Range**	**Mean accuracy**	**Resolution**
Wind speed (RM Young)	0.7–50 m s^{-1}	0.2 m s^{-1} or 2 %	0.1 m s^{-1}
Wind direction (RM Young)	0–360°	3°	1°
Air Temperature (YSI)	0–45°C	0.2°C	0.05°C
Relative Humidity (Rotronic)	0–100%	2 %	0.5 %
Atmospheric Pressure (Honeywell)	850–1050 hPa	0.1 hPa	0.01 hPa
Optical rain gauge (Optical Scientific)	0–50 mm hr^{-1}	0.4 mm hr^{-1}	0.25 mm
Radiation (SW in) (Licor)	0–300 mW cm^{-2}	5 %	—
Sea surface Temperature (Sea Bird)	0–35°C	0.1°	0.05°C

LIST OF FIGURES

Fig. 8. Longitude–depth sections of temperature along 8°N using (a) CTD section during 30 June – 4 July 2016, (b) glider data on 8 July 2016, (c) CTD section observed during 15–20 July 2016, (d) OI Argo data on 24 July 2016. 43

Fig. 9. The SMC. Surface currents from OSCAR (vector, m s^{-1}) overlaid on current speed (shading) on (a) 26 June, (b) 17 July 2016. (c) Trajectories of 4 drifting buoys deployed during the cruise. (d) Meridional geostrophic current referenced to 500 dbar, calculated using ship CTD temperature and salinity measured at every quarter degree longitude along 8°N during 15 – 20 July 2016. (e) Meridional current measured using the ADCP during 30 June - 4 July, and (f) 15–20 July 2016. (g) Time-depth meridional geostrophic current referenced to 500 dbar, at a nominal longitude of 87.5°E, calculated using SG534 and SG532 glider data (Table 1). 44

Fig. 10. High Salinity Core. (a) Vertical section of CTD salinity along 8°N, measured during 30 June - 4 July 2016, at stations located one degree apart between 85.3°E and 89°E. (b) Same section as in (a) profiled during 15-20 July 2016 at stations located a quarter degree longitudes apart. (c) Time-depth section of salinity measured at TSE during 4–15 July 2016. High Salinity (>35) core is highlighted using contours in (a), (b) and (c). (d) Time–longitude section of salinity averaged between 90–130 m using glider data. (e) Time–longitude section of salinity averaged between 90–130 m using Argo data. 45

Fig. 11. Changes in the temperature and salinity characteristics of the upper layer due to freshening. The three upper panels correspond to the first freshening event (4–6 July 2016) described in the text and the three bottom panels correspond to the second (7–13 July 2016). Red, blue, black and gray curves in all panels indicate temperature, salinity, density and MLD respectively. The date and time (UTC) of each profile is given above the respective panel. The left, middle and right panels correspond to the situation before and during the freshening event. The right panel roughly corresponds to the peak of the freshening event. 46

Fig. 12. uCTD observations of a rain-formed low salinity pool. (a) Salinity along a 14 km section over which 21 vertical profiles were measured just after a spell of rain. Locations of uCTD profiles are indicated using asterisks marked at a depth of 55 m. Along the depth axis, the raw data is averaged into 1m bins before plotting.(b) Vertical profiles of temperature (black) and salinity (blue) measured outside the low salinity pool (at $x = 2$ km, thick lines) and inside (at $x = 6$ km, thin lines). 47

Fig. 13. Data from VMP-250 at 7°54'N and 89°06'E on 15 July 2016 : (a) Temperature (blue) and salinity (red). (b) Squared Brunt Vaisala Frequency (N^2, blue) and density (red). (c) $\log_{10}$ of turbulent kinetic energy dissipation rate (ε, blue) and $\log_{10}$ of eddy diffusivity coefficient (K_z, red). Near-simultaneous data from glider SG613: (d) Temperature (blue) and salinity (red). (e) N^2 (blue) and density (red). (f) $\log_{10}$ of ε (blue) and $\log_{10}$ of K_z (red). The noise threshold of $\varepsilon = 10^{-10.5}$ W kg^{-1}. The measured microstructure shear was used to infer ε and K_z in the water column by assuming isotropic turbulence (Moum et al. 1995) and a mixing efficiency of 0.2 (Osborn 1980). The upper 10 m of the VMP-250 data has been removed to avoid contamination by the ship's wake. 48

Fig. 14. PAR profile (black dots) from a sample dive from glider SG579, near midday on 6 July 2016. The best fit double exponential curve is shown by the black line. Chlorophyll concentration is shown by the green crosses and line. 49

Fig. 15. Spatial variation of surface biogeochemical properties during BoBBLE: (a) dissolved oxygen, (b) pH, (c) total alkalinity, (d) atmospheric pCO_2^{air}, pCO_2^{sw} in sea water and the difference in air-sea pCO_2 concentration. Water sampling was carried out using a Seabird

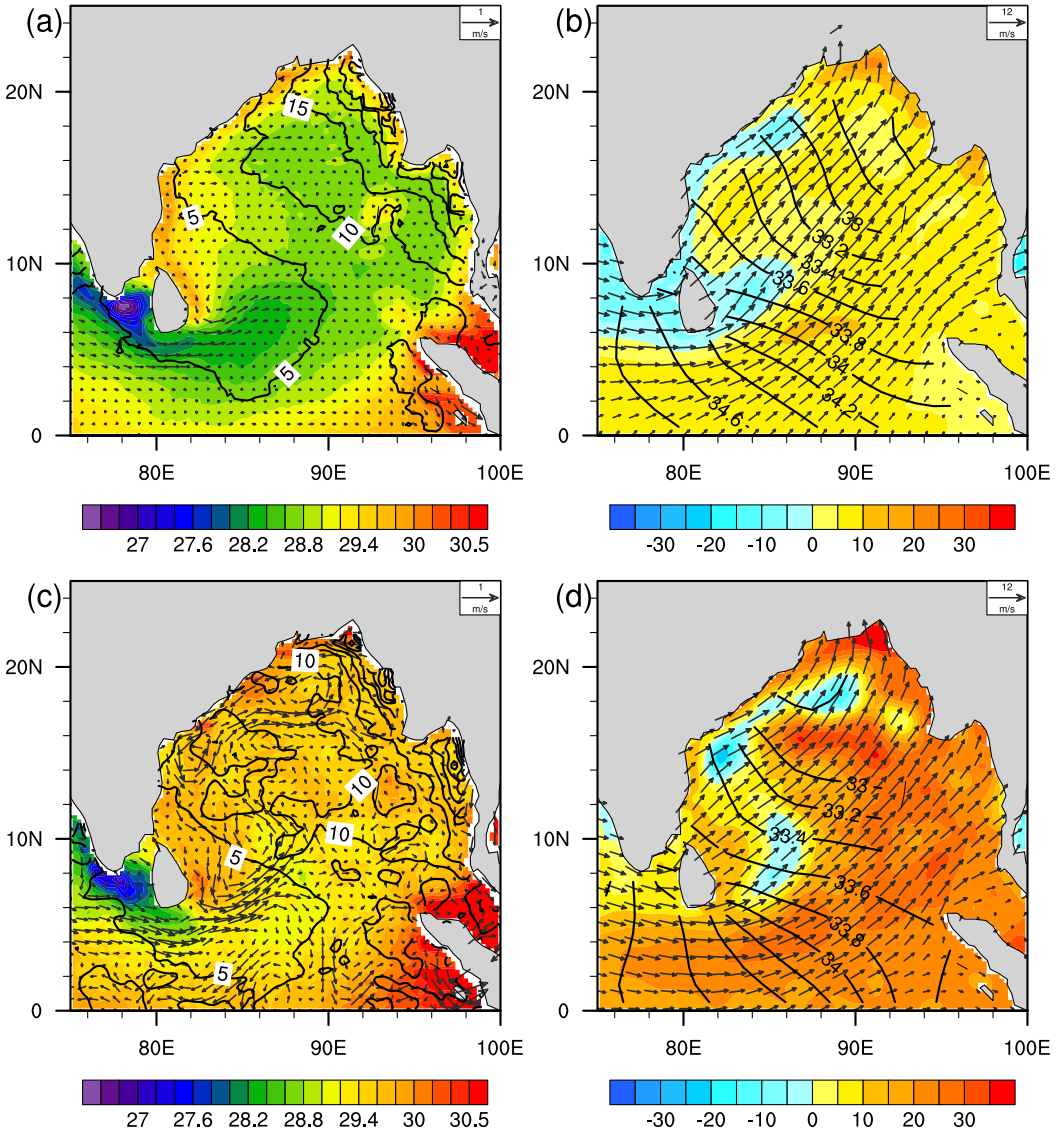

665 FIG. 1. Climatology for the period 23 June – 24 July. (a)TMI SST (1998–2014, shading in °C), TRMM
666 rainfall (1998–2015, contours) OSCAR (1993–2015, vector arrows); (b) AVISO MSLA (1993–2015, shading
667 in cm), salinity from Argo (2005–2015, contours) ASCAT surface winds (2008–2015, vector arrows). Fields in
668 panels (c) and (d) are the same as in panels (a) and (b), respectively, except that they are for the period 23 June -
669 24 July, 2016

FIG. 2. *RV Sindhu Sadhana* of CSIR-National Institute of Oceanography, Goa, India which was used for the BoBBLE field program.

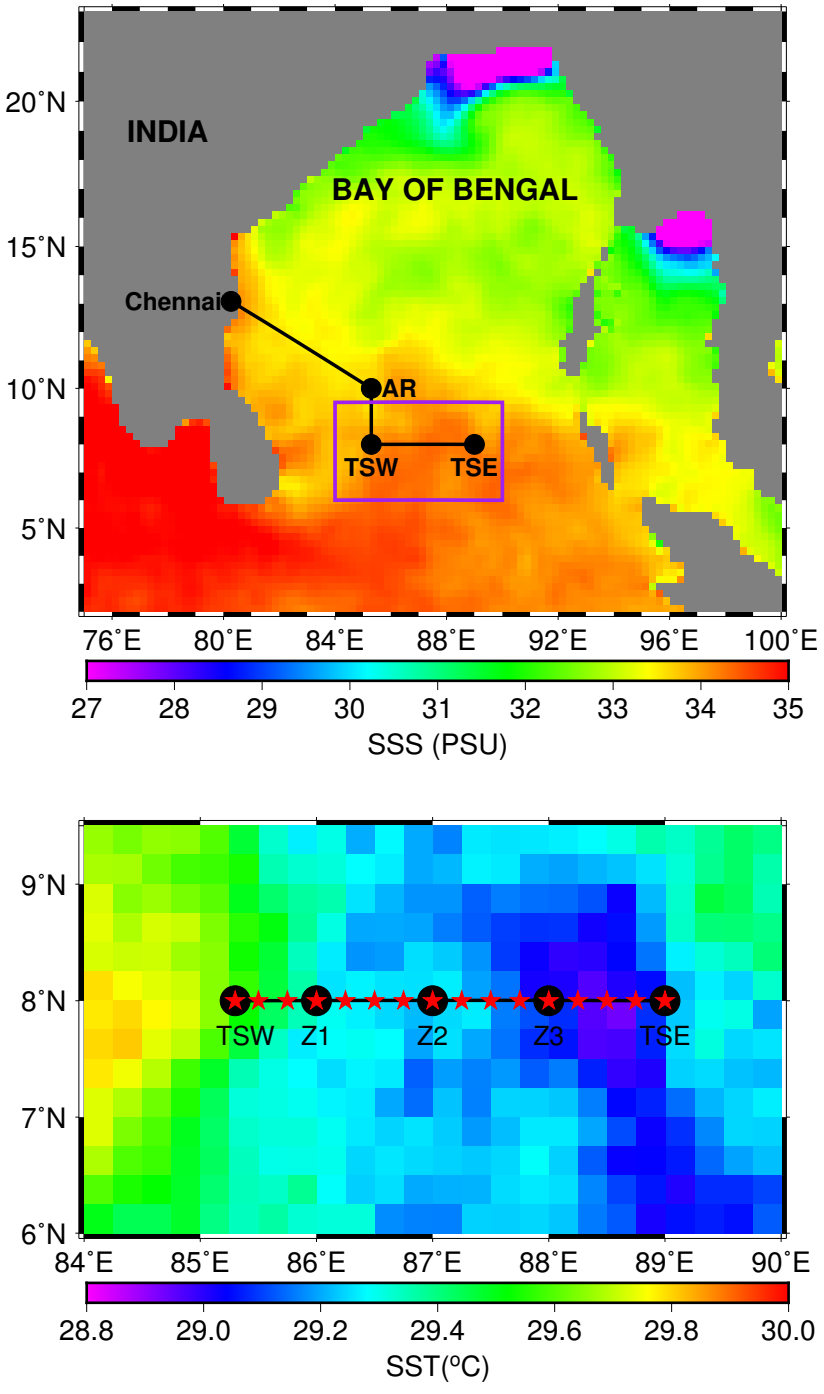

672 FIG. 3. Upper panel: a map of the BoB and the cruise track of the BoBBLE field program. Shading is
673 SSS from SMAP. Lower panel: The section along which observations were made during BoBBLE. The black
674 circles (TSW, Z1, Z2, Z3 and TSE) represent glider deployment locations (see Table 1 for details). Argo float
675 deployments (see Table 2 for details), IOP, radiometer and VMP profiling as well as water sampling were also
676 carried out at these locations. Stars indicate locations where additional CTD profiles were measured during the
677 return leg of the cruise. At TSE, additionally, CTD profiles were measured from 4 to 15 July 2016. Shading
678 indicates SST from AMSR-E.

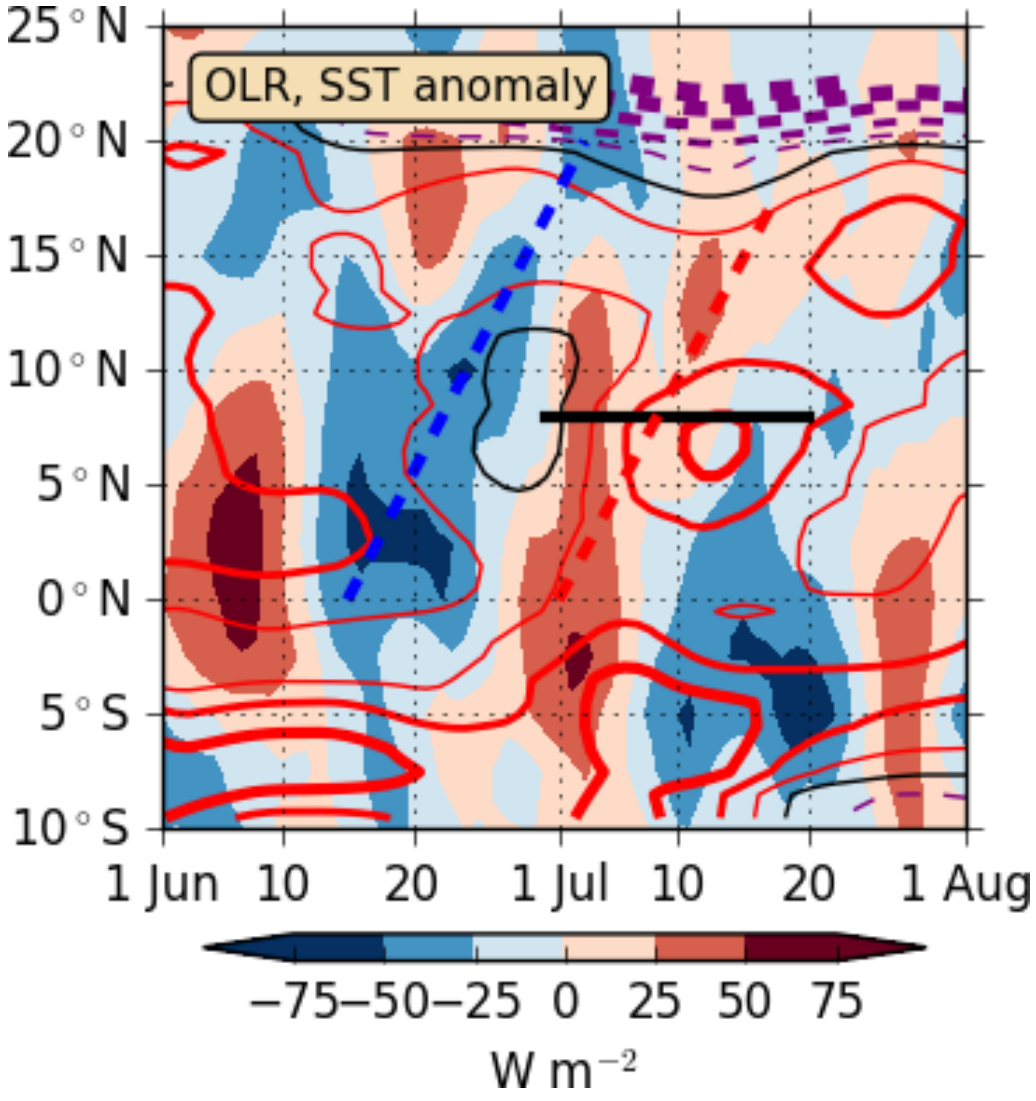

679 FIG. 4. Hovmöller diagram (averaged from 80°-95°E) for anomalous 5-day running mean OLR (shading
680 interval 25 W m^{-2}), SST (line contour interval 0.2°C; negative contours dashed purple, zero contour solid
681 black, positive contours solid red). The solid black line at 8°N shows the timing of the BoBBLE ship and glider
682 and Argo float deployments. Negative (positive) OLR anomalies indicate convectively active (suppressed) phase
683 of BSISO. The dashed blue (red) lines are shown to subjectively indicate the main axis of northward propagation
684 of the active (suppressed) phases of the BSISO during June-July 2016.

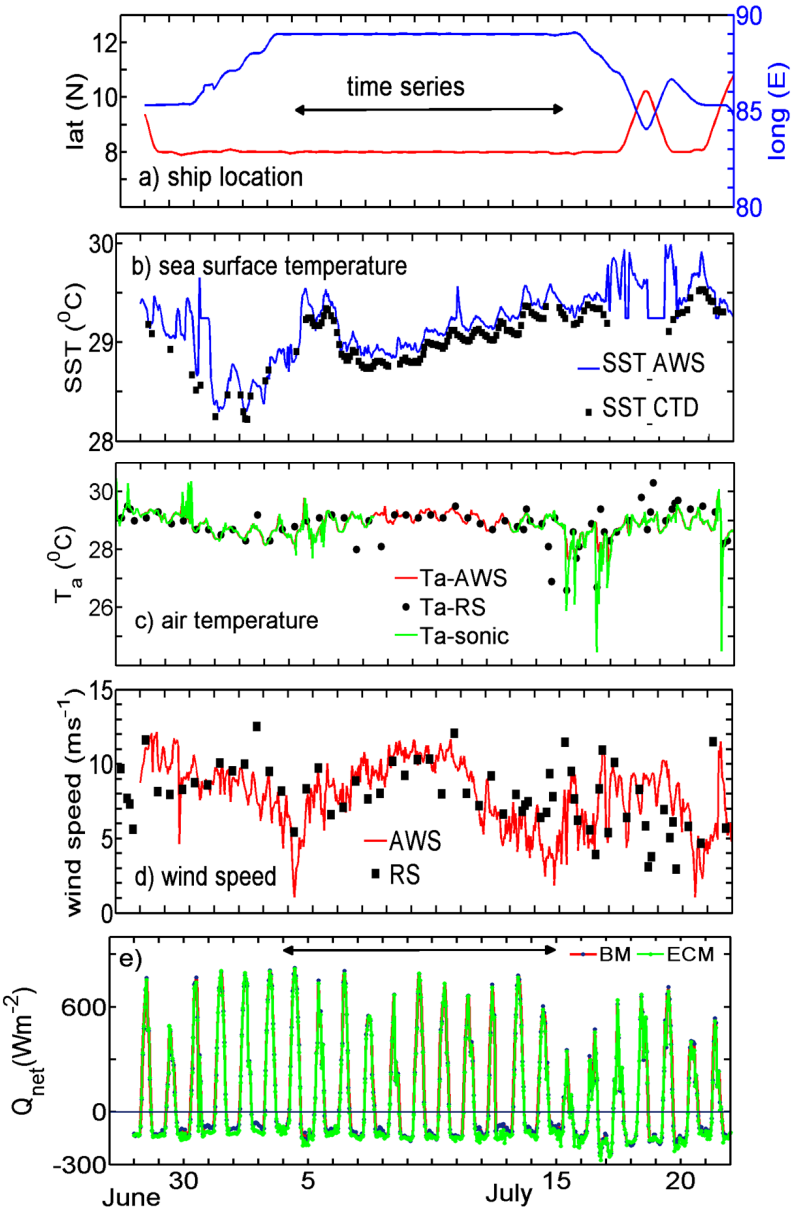

FIG. 5. (a) Ship position as a function of time. Red and dark blue lines correspond to latitude and longitude respectively. The double-headed arrow shows the time series observation period at TSE (89°E, 8°N). (b) SST from AWS and CTD at 3.4 m depth. (c) Air temperature. (d) Surface (approximately 10 m) wind speed (red line,) and radiosonde wind speed (black squares) at 975 hPa. (e) Surface net heat flux into the ocean. The text in the legends corresponds to: AWS - automatic weather system; CTD - conductivity, temperature and depth probe; RS - radiosonde; Ta_sonic - sonic anemometer temperature corrected for water vapor; ECM and BM refer to turbulent fluxes calculated using the eddy covariance and bulk methods, respectively.

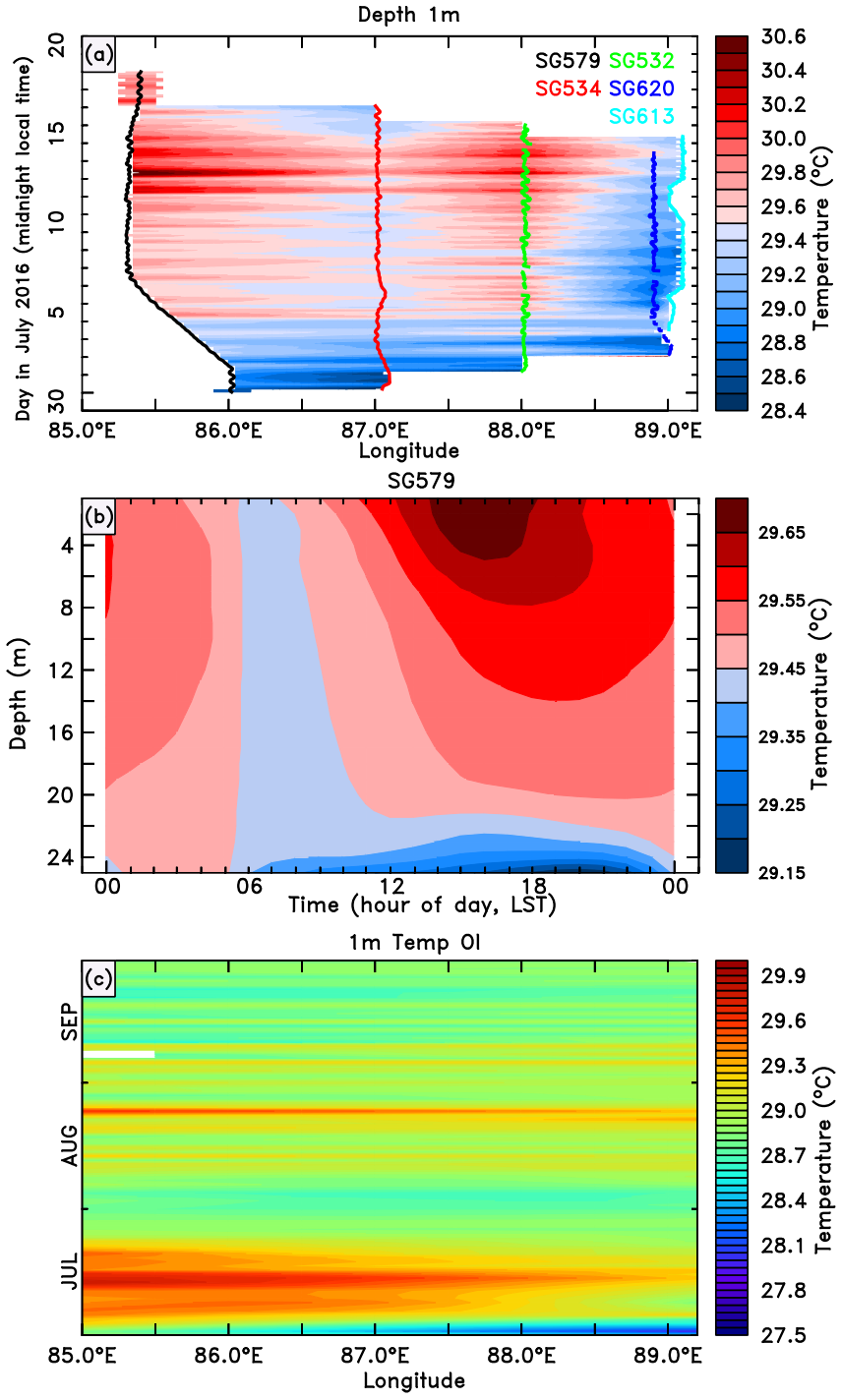

692 FIG. 6. (a) Longitude–time section of OI glider temperature at 1 m depth. The longitudes of the five gliders
693 are shown by the coloured lines. (b) Average diurnal cycle of temperature for glider SG579 at the western end
694 of the 8°N section. Time of day is in local solar time (LST). (c) Longitude–time section of temperature at 1
695 m depth for the July–September months of 2016, based on OI Argo data. A three day moving mean has been
696 applied to the Argo data.

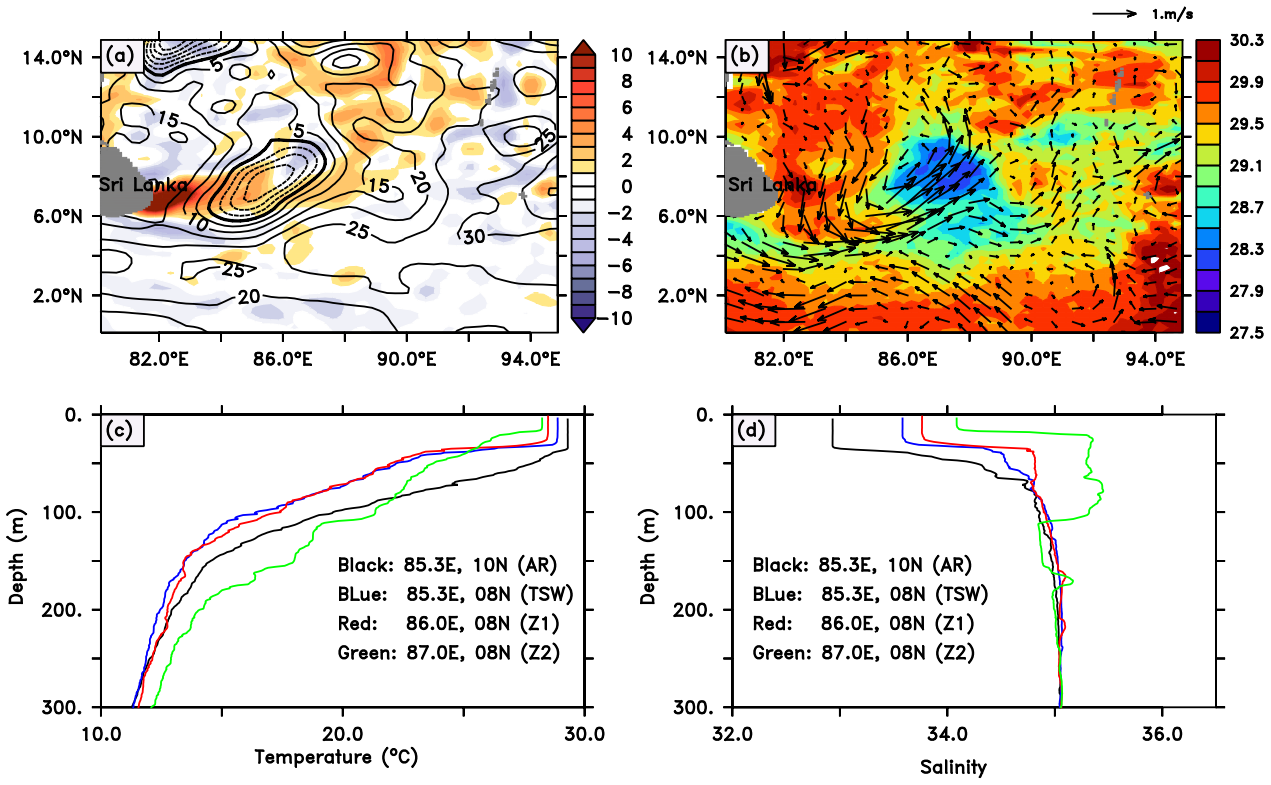

FIG. 7. Sri Lanka dome. (a) AVISO MSLA (cm) for 30 June 2016 (contours) and wind stress curl (shading, N m^{-3}) from ASCAT averaged for the period 20 June - 1 July 2016. (b) AMSR-E SST (shading, °C) averaged for the period 27 - 30 June 2016 overlayed on current vectors (m s^{-1}) from OSCAR for 2 July 2016. (c) Temperature and (d) salinity profiles that contrasts the spatial structure of the SLD. Profiles in black and green were measured at a location to the north and east of the SLD respectively, and those in blue and red were measured inside the SLD. Refer to Fig. 3 for the locations. Salinity profiles shows that the high salinity core of the SMC (green curve) is absent in the regions of SLD (blue and red).

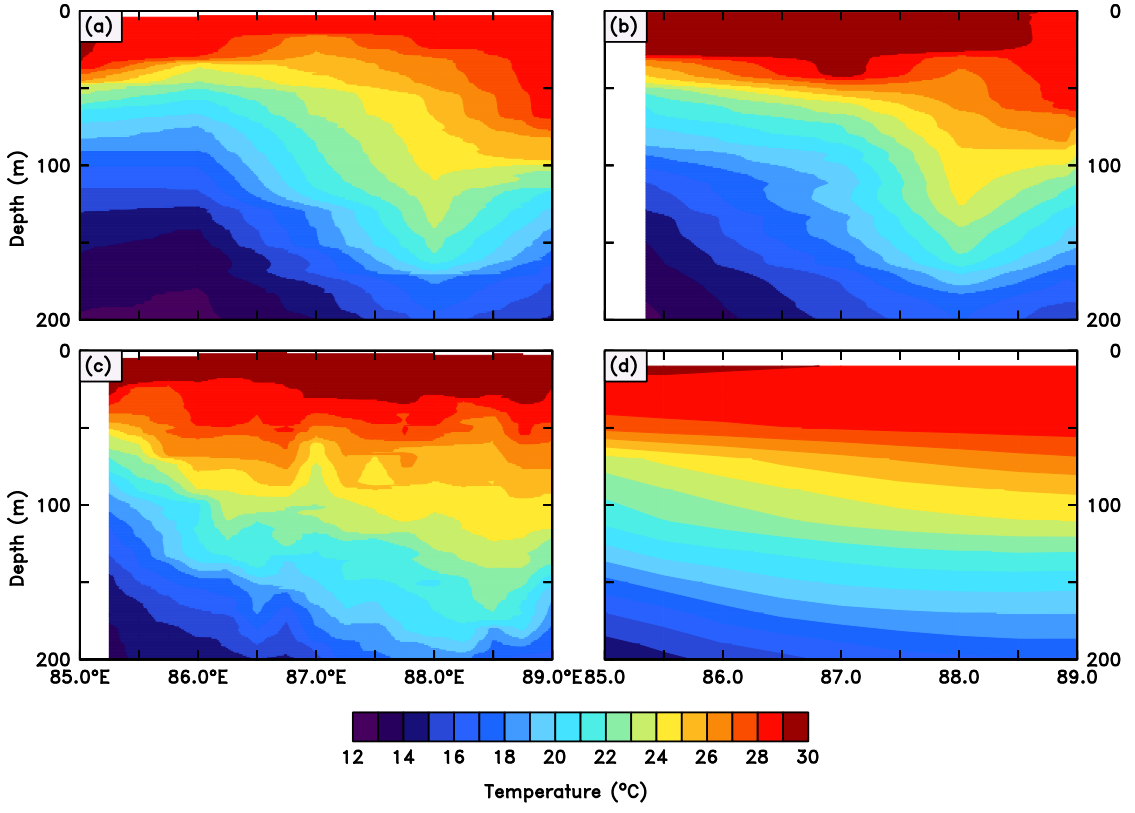

704 FIG. 8. Longitude–depth sections of temperature along 8°N using (a) CTD section during 30 June – 4 July
705 2016, (b) glider data on 8 July 2016, (c) CTD section observed during 15–20 July 2016, (d) OI Argo data on 24
706 July 2016.

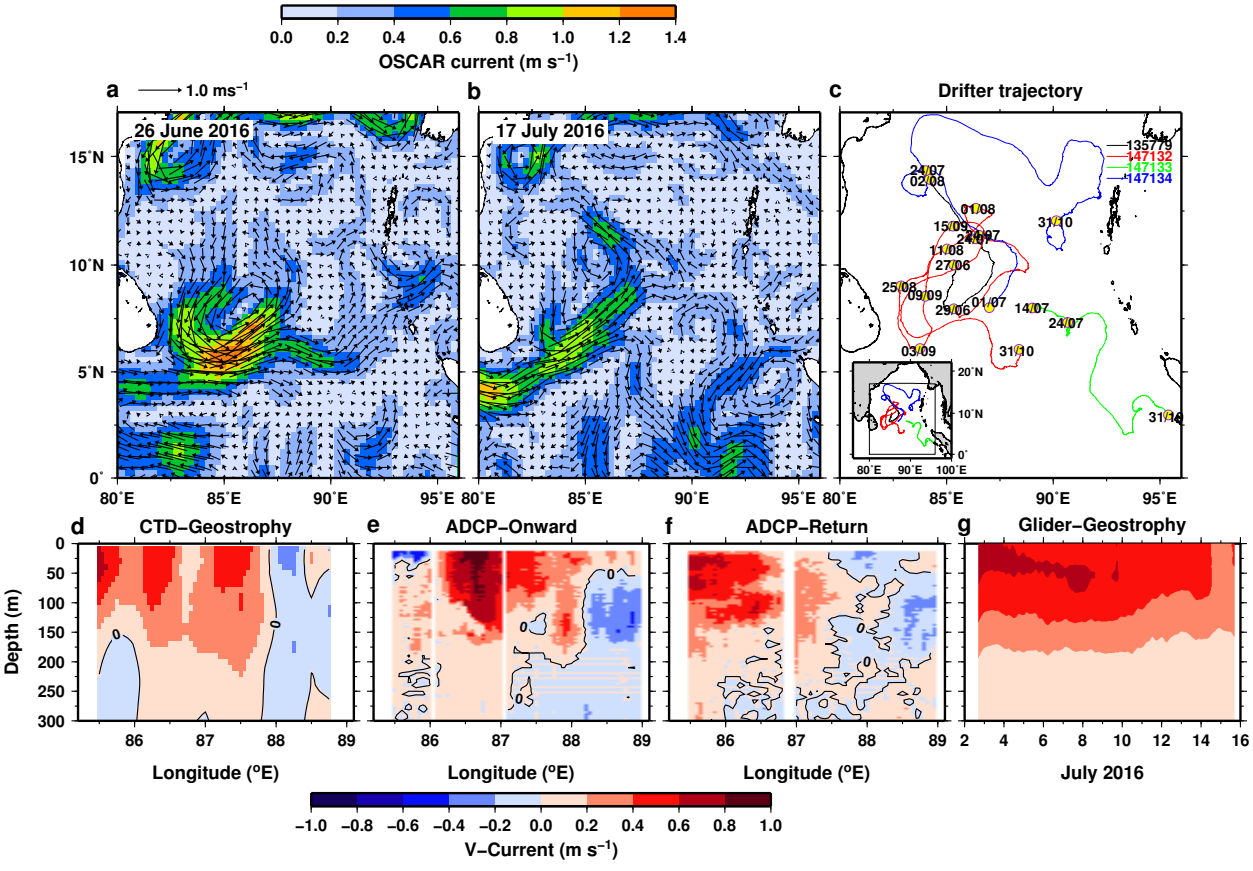

FIG. 9. The SMC. Surface currents from OSCAR (vector, m s^{-1}) overlaid on current speed (shading) on (a) 26 June, (b) 17 July 2016. (c) Trajectories of 4 drifting buoys deployed during the cruise. (d) Meridional geostrophic current referenced to 500 dbar, calculated using ship CTD temperature and salinity measured at every quarter degree longitude along 8°N during 15 – 20 July 2016. (e) Meridional current measured using the ADCP during 30 June - 4 July, and (f) 15–20 July 2016. (g) Time-depth meridional geostrophic current referenced to 500 dbar, at a nominal longitude of 87.5°E, calculated using SG534 and SG532 glider data (Table 1).

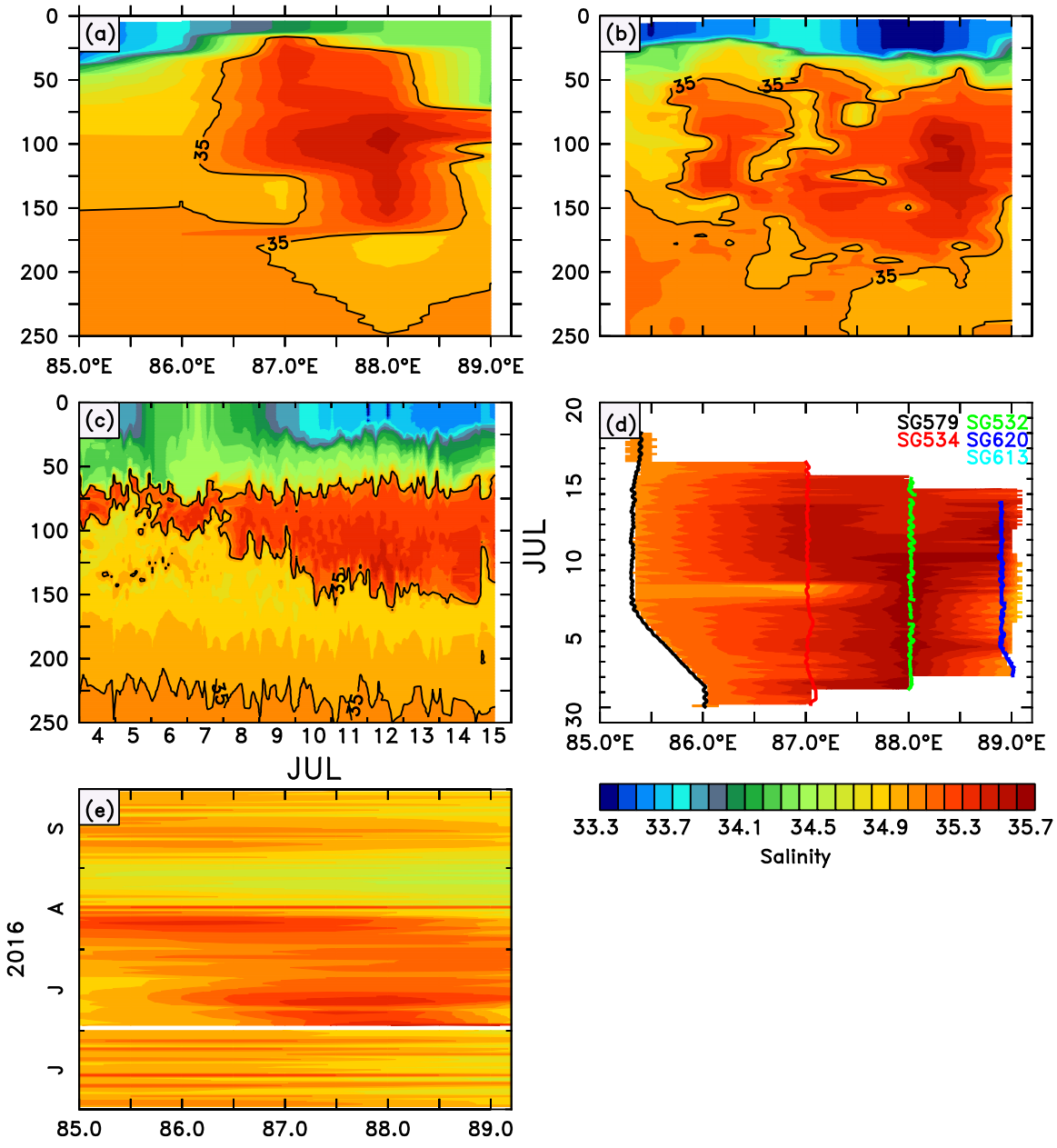

FIG. 10. High Salinity Core. (a) Vertical section of CTD salinity along 8°N, measured during 30 June - 4 July 2016, at stations located one degree apart between 85.3°E and 89°E. (b) Same section as in (a) profiled during 15-20 July 2016 at stations located a quarter degree longitudes apart. (c) Time-depth section of salinity measured at TSE during 4–15 July 2016. High Salinity (>35) core is highlighted using contours in (a), (b) and (c). (d) Time–longitude section of salinity averaged between 90–130 m using glider data. (e) Time–longitude section of salinity averaged between 90–130 m using Argo data.

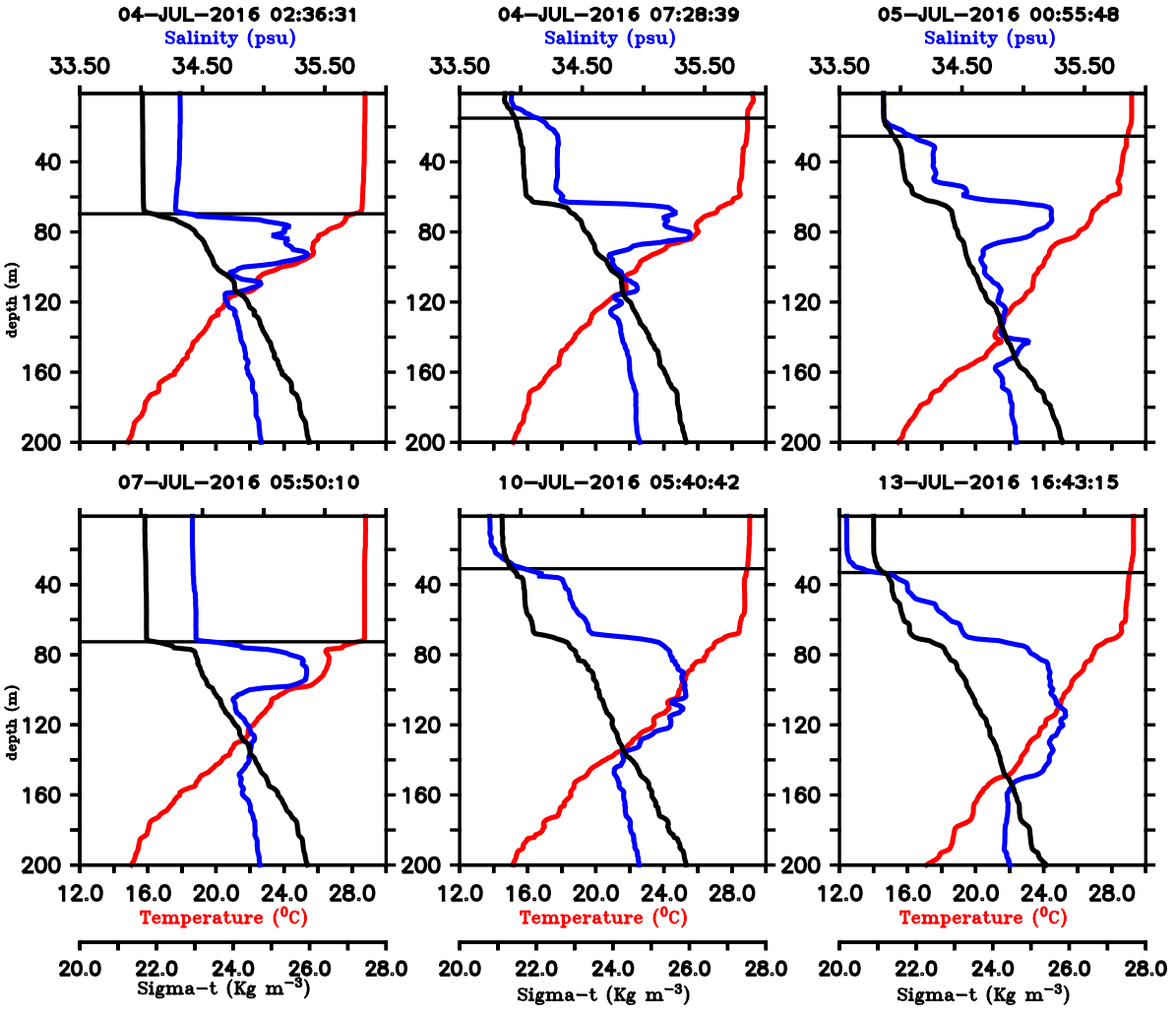

719 FIG. 11. Changes in the temperature and salinity characteristics of the upper layer due to freshening. The
720 three upper panels correspond to the first freshening event (4–6 July 2016) described in the text and the three
721 bottom panels correspond to the second (7–13 July 2016). Red, blue, black and gray curves in all panels indicate
722 temperature, salinity, density and MLD respectively. The date and time (UTC) of each profile is given above the
723 respective panel. The left, middle and right panels correspond to the situation before and during the freshening
724 event. The right panel roughly corresponds to the peak of the freshening event.

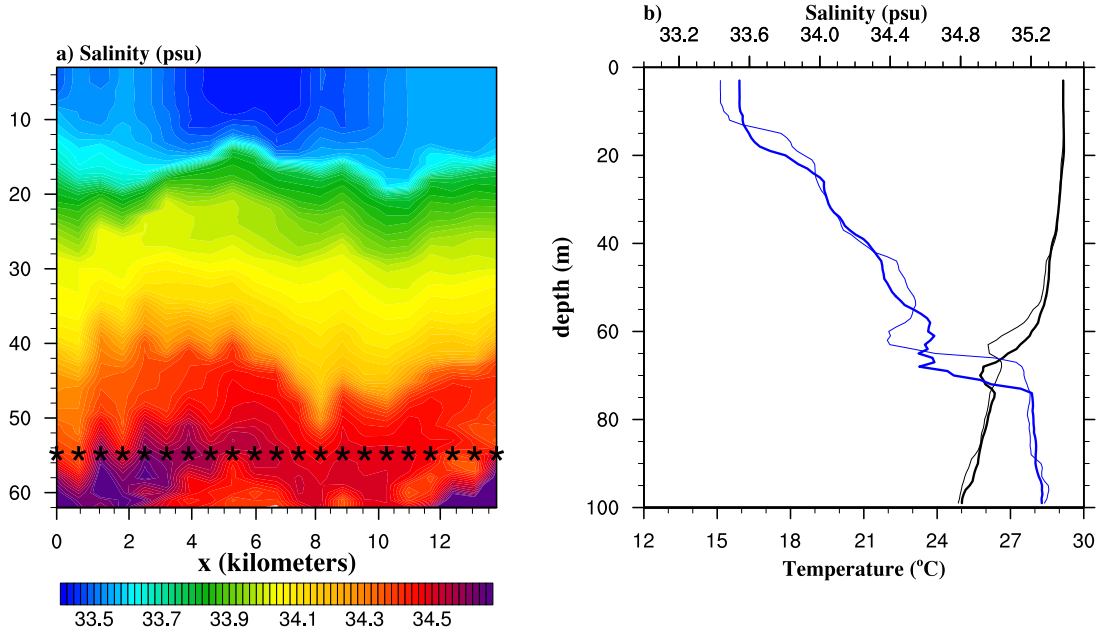

725 FIG. 12. uCTD observations of a rain-formed low salinity pool. (a) Salinity along a 14 km section over
726 which 21 vertical profiles were measured just after a spell of rain. Locations of uCTD profiles are indicated
727 using asterisks marked at a depth of 55 m. Along the depth axis, the raw data is averaged into 1m bins before
728 plotting.(b) Vertical profiles of temperature (black) and salinity (blue) measured outside the low salinity pool (at
729 $x = 2$ km, thick lines) and inside (at $x = 6$ km, thin lines).

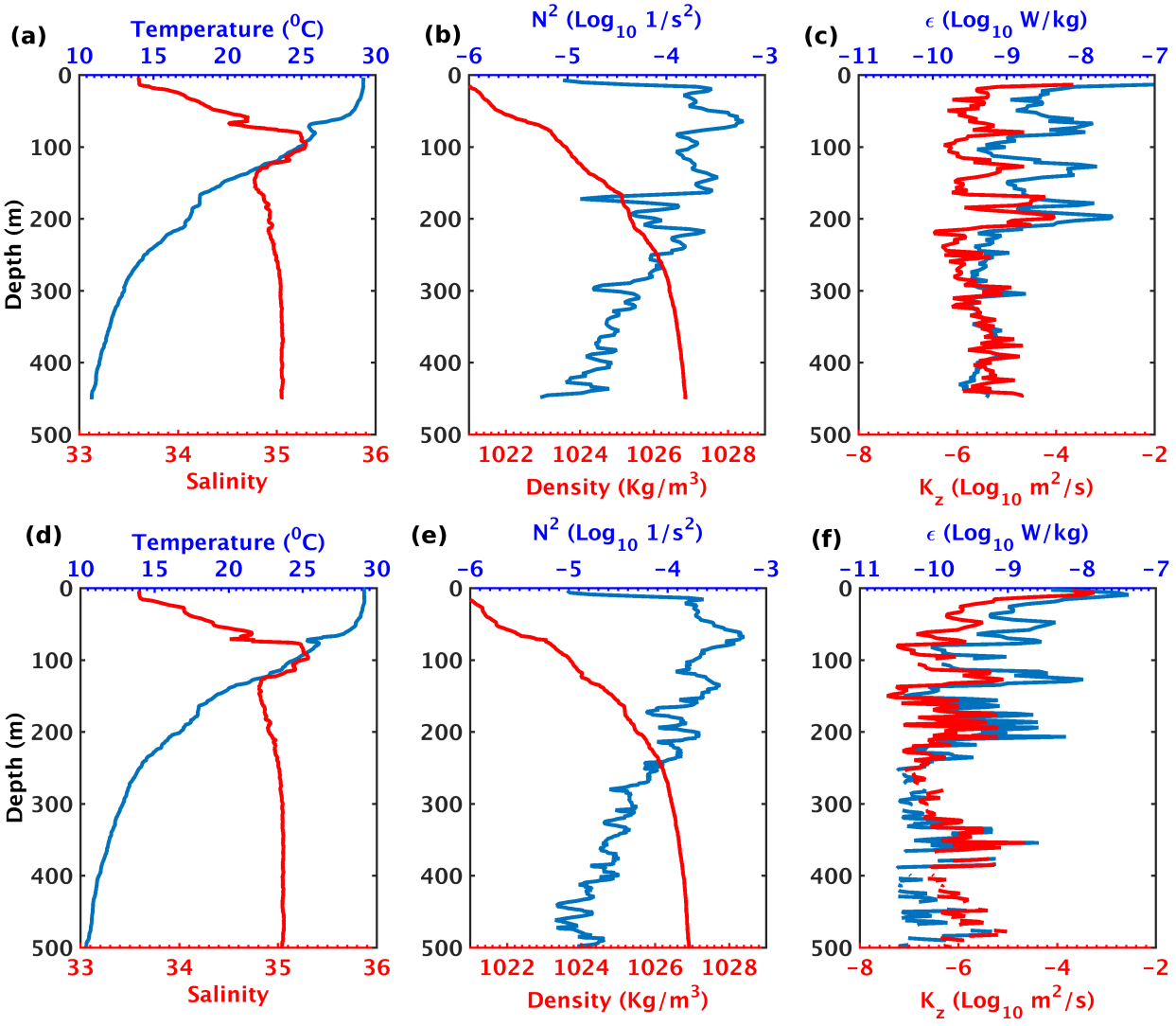

730 FIG. 13. Data from VMP-250 at 7°54'N and 89°06'E on 15 July 2016 : (a) Temperature (blue) and salinity
731 (red). (b) Squared Brunt Vaisala Frequency (N^2, blue) and density (red). (c) $\log_{10}$ of turbulent kinetic energy
732 dissipation rate (ε, blue) and $\log_{10}$ of eddy diffusivity coefficient (K_z, red). Near-simultaneous data from glider
733 SG613: (d) Temperature (blue) and salinity (red). (e) N^2 (blue) and density (red). (f) $\log_{10}$ of ε (blue) and $\log_{10}$
734 of K_z (red). The noise threshold of $\varepsilon = 10^{-10.5}$ W kg^{-1}. The measured microstructure shear was used to infer ε
735 and K_z in the water column by assuming isotropic turbulence (Moum et al. 1995) and a mixing efficiency of 0.2
736 (Osborn 1980). The upper 10 m of the VMP-250 data has been removed to avoid contamination by the ship's
737 wake.

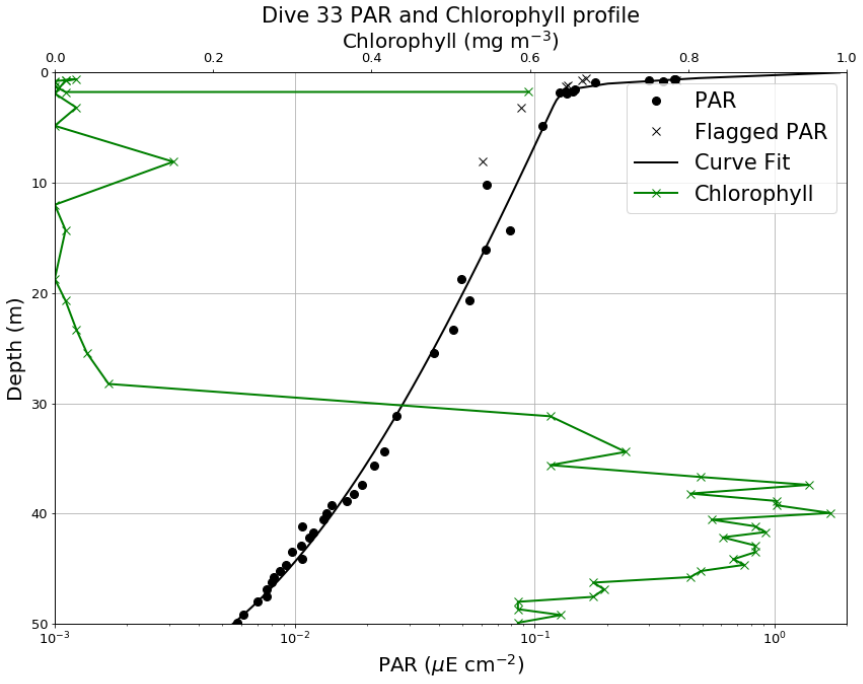

738 FIG. 14. PAR profile (black dots) from a sample dive from glider SG579, near midday on 6 July 2016. The
739 best fit double exponential curve is shown by the black line. Chlorophyll concentration is shown by the green
740 crosses and line.

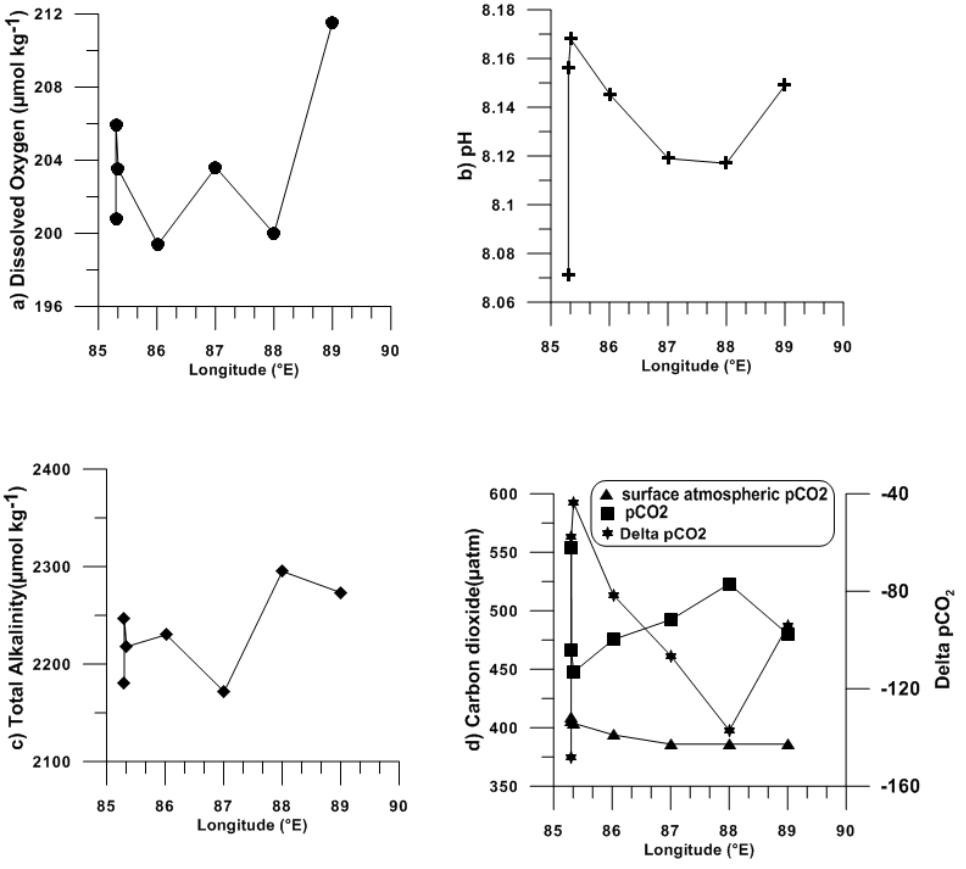

741 FIG. 15. Spatial variation of surface biogeochemical properties during BoBBLE: (a) dissolved oxygen, (b)
742 pH, (c) total alkalinity, (d) atmospheric pCO_2^{air}, pCO_2^{sw} in sea water and the difference in air-sea pCO_2 con-
743 centration. Water sampling was carried out using a Seabird CTD–rosette system fitted with 10 L Niskin bottles.
744 Samples were collected along the 8°N transect at locations denoted by the red stars in Fig. 3.